

Detectability of Prompt TeV Gamma Rays of Proton Synchrotron Origin from Gamma Ray Bursts by AMANDA/ICECUBE Detectors

Pijushpani Bhattacharjee¹

Indian Institute of Astrophysics, Bangalore 560 034, INDIA.

Nayantara Gupta²

*Department of Theoretical Physics,
Indian Association for the Cultivation of Science,
Jadavpur, Calcutta 700 032, INDIA.*

Abstract

The detectability of a possible “high” energy ($> 100 \text{ GeV}$) component of Gamma-Ray Bursts (GRBs) using AMANDA/ICECUBE large area muon detectors is examined within the context of a specific model of such high energy gamma ray production within GRBs, namely, the proton-synchrotron model, which requires protons to be accelerated to ultrahigh energies $\gtrsim 10^{20} \text{ eV}$ within GRBs. In this model, the high energy component is distinct from, but may well be emitted in coincidence with, the usual “low” (keV–MeV) energy component observed by satellite-borne detectors. The AMANDA/ICECUBE detectors can detect TeV photons by detecting the secondary muons created by the TeV photons in the Earth’s atmosphere. We calculate the muon signal to noise ratio in these detectors due to TeV gamma-rays from individual GRBs for various assumptions on their luminosity, distance (redshift), Lorentz Gamma factor of the underlying fireball model, and various spectral characteristics of the GRBs, including the effect of the absorption of TeV photons within the GRB as well as in the intergalactic infrared radiation background. The intergalactic absorption effect essentially precludes detection of TeV photons in the AMANDA detector for reasonable values of the luminosity in the high energy component, but they may well be detectable in the proposed ICECUBE detector which may have an effective area for downward-going muons a factor of 100 larger than that in AMANDA. However, even in ICECUBE, only relatively close-by GRBs at redshifts < 0.05 or so can be expected to be detectable with any reasonable degree of confidence. We discuss the requirement on the luminosity of the GRB in the high energy component for its detectability in ICECUBE.

¹pijush@iiap.ernet.in

²tpng@mahendra.iacs.res.in

1 Introduction

Gamma Ray Bursts (GRBs), short and intense bursts of photons observed mostly in the energy range of few tens of keV to few MeV with burst duration lasting from fraction of a second to several hundreds of seconds (see e.g., Ref. [1] for a review), are one of the most powerful and enigmatic astrophysical phenomena in the Universe. An afterglow phase, lasting from several hours to several days, has also been detected for many bursts. Detections of these afterglow phases in optical and/or x-rays and in some cases in radio, have provided valuable information regarding the nature of GRBs [2]. For example, large redshifts of the host galaxies of some GRBs, measured from observations of their optical afterglows, have unambiguously established that GRB sources are extragalactic and indeed lie at cosmological distances.

The total energy emitted in a GRB, estimated from the observed fluence and measured redshift (distance) of the burst source assuming isotropic emission, varies over a wide range from burst to burst, from about few $\times 10^{50}$ ergs to $\sim 10^{54}$ ergs. On the other hand, the material emitting the radiation could itself be highly collimated in the form of a jet, making the emitted radiation highly non-isotropic. One possible diagnostic, albeit not always a robust one, of a collimated emission is an expected break feature [3] in the light curve of the optical afterglow of the GRB. Collimated emission significantly reduces the estimated total energy of the burst compared to that estimated assuming isotropic emission. From an analysis of the measured redshift and estimated collimation angle (from the break feature in the optical afterglow light curve) of some 18 bursts, Ref. [4] finds a rather narrow distribution of the total energies of bursts with typical values around 5×10^{50} ergs with a FWHM of a factor of ~ 5 .

The satellite-borne detectors, such as the BATSE on board the Compton Gamma Ray Observatory (CGRO) and earlier detectors on board the Vela series of satellites, have detected GRBs mostly in the sub-MeV energy region. However, several GRBs with emission beyond 100 MeV, and in coincidence with the sub-MeV burst, have been detected [5, 6, 7] by the EGRET instrument on board the same CGRO, including the long-duration burst GRB940217 [6] with emission extending to ~ 18 GeV. This suggests the possibility that GRBs may, in addition to the sub-MeV photons, also emit much higher energy photons, perhaps even extending to TeV energies as in some highly energetic Active Galactic Nuclei. For power-law spectra falling with energy, the photon number flux at TeV energies may be too low for these more energetic photons from GRBs to be detected by the satellite-borne detectors which have limited sizes. However, ground-based detectors can in principle detect TeV photons from GRBs by detecting the secondary particles comprising the “air showers” generated by these photons in the Earth’s atmosphere.

Indeed, three major ground-based gamma ray detectors, the Tibet air shower array [8], the HEGRA-AIROBICC Cherenkov array [9] and the Milagro water-Cherenkov detector [10] have independently claimed evidence, albeit not with strong statistical significance, for possible TeV γ -ray emission from sources in directional and temporal coincidence with some GRBs detected by BATSE. The estimated energy in TeV photons in each case has been found to be about 1 to 2 orders of magnitude larger than the corresponding sub-MeV energies measured by BATSE. More recently, a search [11] for sub-TeV (> 10 GeV) gamma rays from GRBs with the Project GRAND array of muon detectors reported one possible detection at the 2.7σ level in coincidence with one BATSE GRB (971110), and an analysis [12] of the energetics of this event within the context of various possible models of TeV gamma ray emission from GRBs indicates a significantly higher estimated energy in TeV photons (by four orders of magnitude or more) than in sub-MeV photons.

Note that, since TeV photons are efficiently absorbed in the intergalactic infrared (IR) background due to pair production [13], only relatively close by (i.e., low redshift) GRBs, for which the absorption due to IR background is insignificant, can be observed at TeV energies, which would explain the fact that only a few of the BATSE-detected GRBs in the fields of view of the individual ground detectors have been claimed to be detected at TeV energies.

The significantly higher total energies estimated for the TeV photon emitting GRBs claimed to be detected by the ground-based detectors mentioned above raise the possibility that the TeV photons may constitute a separate ‘high’ (GeV–TeV) energy component of GRB emission distinct from the ‘low’ (keV–MeV) energy component detected by BATSE. For, otherwise, if the ‘observed’ TeV photons came from the same low energy spectrum continued to TeV energies, then it would be difficult to understand the significantly higher total energy estimated for the bursts from the TeV observations than that estimated for the same bursts from sub-MeV observations by BATSE detector, unless the spectrum is hard with a differential power-law spectrum, $dN/dE \propto E^{-\alpha}$, with $\alpha < 2$, which is not the case for the observed bursts.

Confirmation of TeV gamma ray emission from GRBs would have major implications not only for the physics and astrophysics of GRBs as such, but also for several other phenomena. For example, some of the proposed mechanisms [14, 15, 16, 17] of possible TeV photon emission from GRBs discussed below are directly linked with the proposed scenario of GRBs being possible sources of Ultrahigh Energy Cosmic Rays (UHECR) [18]. It has also been suggested [19, 20] that while the TeV photons emitted by GRBs at large redshifts would be absorbed through e^+e^- pair production on the intergalactic infrared background, the resulting electromagnetic cascades initiated by the produced pairs could produce the observed extragalactic diffuse gamma

ray background in the GeV energy region. It is, therefore, important to study the detectability of the possible TeV photon emissions from GRBs in as many different ways as possible.

In this paper, we study the detectability of possible TeV photons from GRBs in the proposed ICECUBE [21] class underground muon detectors, within the context of a specific model of such high energy gamma ray production within GRBs, namely, the proton-synchrotron model discussed in detail below. The ICECUBE type muon detectors can detect TeV photons through detection of the secondary muons that are produced in Earth’s atmosphere by high energy photons of energy above a few hundred GeV.

The ICECUBE is the proposed full-scale version of the already operating AMANDA [22] detector. These are facilities primarily for detecting high energy neutrinos from cosmic sources. Located under the antarctic ice sheet, and consisting of arrays of photomultiplier tubes (PMTs) attached to strings and frozen in the deep ice, these detectors detect high energy neutrinos by detecting the muons produced by the neutrinos within the detector volume in the ice; the muons themselves are detected and their tracks (and thereby the arrival direction of the parent neutrinos) reconstructed using the array of PMTs which register the cherenkov light emitted by the muons traveling through the ice. In the final analysis, however, these are just muon detectors, and can, in principle, also detect the muons produced by TeV photons in the Earth’s atmosphere. There is one basic difference, though, in the detection method employed for photons as against that for neutrinos: While for neutrinos one looks for upward-going muons in the detector, photons have to be detected only through detection of the downward-going muons in the detector.

The advantages of using these muon detectors over the conventional air-Cherenkov telescopes for doing TeV gamma ray astronomy have been expounded in Refs. [23, 24]. Compared to air-Cherenkov telescopes, these detectors typically cover much larger fraction of the sky with large duty cycles. For example, the AMANDA detector covers more than a quarter of the sky with essentially 100% efficiency. The detector is sensitive to muons with energies of a few hundred GeV and thereby to parent photons of energy of order a TeV and above. The fact that air-showers created by gamma rays are relatively “muon poor” (as compared to air-showers generated by hadrons) can be, to a large extent, compensated for by the relatively large effective area of a detector such as ICECUBE ($\sim 1 \text{ km}^2$). In addition, as pointed out in Ref. [24] (AH, hereafter), despite the otherwise large background of down-going cosmic-ray induced atmospheric muons, the above muon detectors can in principle detect TeV gamma rays from transient sources like GRBs because, with the information on the time and duration of a burst provided by satellite observation, the background is significantly

reduced because it is integrated only over the relatively short duration of a typical GRB which is of order few seconds.

Of course, possible TeV photons from GRBs can be detected by “conventional” air-shower detectors, as exemplified by the claimed detections [8, 9, 10] already mentioned above. In this paper we focus on the AMANDA/ICECUBE detectors for the advantages mentioned above and in particular for their potentially unique capability of simultaneously being detectors of neutrinos as well as photons of TeV energy and above, albeit not from the same source.

In AH [24], the expected number of muons and the signal-to-noise ratios in AMANDA and Lake Baikal detectors due to TeV gamma-rays from individual GRBs were calculated for various different values of the GRB parameters. AH assumed a *single* power-law energy spectrum for individual GRBs continuing from the MeV BATSE band to TeV energies. However, as discussed above, it is more likely that the TeV photons constitute a separate high energy component distinct from the low energy “BATSE” component. In this paper, therefore, we consider such a model of TeV gamma ray emission from GRBs, namely, the proton-synchrotron model, in which, the TeV photons come from a new component different in origin than the sub-MeV “BATSE” photons. We study the detectability of the TeV photons in AMANDA/ICECUBE detectors within the context of this model, and study the sensitivity of the signal-to-noise ratio to various parameters such as the total luminosity of the GRB in the high energy (GeV–TeV) component, the redshift of the burst, etc., and in particular, the Lorentz Gamma factor (Γ) of the ultra-relativistic wind in the underlying fireball model (see below) of the GRB.

The rest of this paper is organized as follows: In Sec. 2, we briefly discuss the motivation for considering the specific model of TeV photon production in GRBs in this paper, namely, the proton synchrotron model. The model is discussed in detail in Sec. 3. The internal optical depth of the produced high energy photons due to the process $\gamma\gamma \rightarrow e^+e^-$ within the GRB environment is calculated in detail in Sec. 4 giving the spectrum of high energy photons escaping from the GRB source. We also give the expression for the spectrum of photons arriving at Earth which includes the effect of the intergalactic absorption of TeV photons due to the process $\gamma\gamma \rightarrow e^+e^-$ taking place on the photons constituting the intergalactic infrared background. In Sec. 5, the parametrization of the number of secondary muons in photon-induced showers in Earth’s atmosphere used in this paper is discussed, and the muon signal-to-noise ratio in a ICECUBE class detector is calculated for individual GRBs as functions of various GRB parameters. The main results are discussed in Sec. 6, and conclusions are presented in Sec. 7.

2 Mechanisms of TeV Gamma Ray Production in GRBs: Motivation for Proton-Synchrotron Mechanism

The fundamental source of the radiation from GRBs is thought to be the dissipation of the kinetic energy of ultra-relativistic (Lorentz factor $\Gamma \gtrsim \text{few } 100$) bulk flow of matter caused by emission from a central engine, the nature of which is not yet known. Ultra-relativistic bulk flow of matter is obtained naturally in the fireball model (see. e.g., [25] for reviews), in which the central engine initially releases a large amount of thermal energy E_{th} mostly in the form of an electron-positron-photon plasma in a small volume in a relatively baryon dilute medium. The baryon load — consisting of the baryons emitted by the central engine as well as those present in the ambient medium — is assumed to be small, i.e., $\eta^{-1} \equiv Mc^2/E_{\text{th}} \ll 1$, where M is the total mass of the baryon load. Because of the high optical depth of the photons due to the pair production process $\gamma\gamma \rightarrow e^+e^-$, the photons cannot escape; instead, the radiation pressure pushes the baryons into a shell of matter that expands outward. The initial thermal energy of the fireball thus gets transferred to the kinetic energy of an expanding shell of matter which, because of its small baryonic load, eventually attains Lorentz factor $\Gamma \sim \eta \gg 1$ when essentially all of the initial thermal energy of the fireball is converted to kinetic energy of bulk flow. If the emission from the central engine is unsteady and sporadic, then the above process may result in multiple shells of baryons moving with different lorentz factors, whereas a single ultrarelativistic baryonic shell is obtained if the emission from the central engine is steady over the duration of the emission. In either case, the observed radiation is believed to arise from reconversion, through some dissipative process, of the kinetic energy of the ultra-relativistic bulk flow of matter back to internal energy at a large radius beyond the “Thomson photosphere” where the optical depth due to pair production, Thomson scattering and other processes is small.

The dissipation of kinetic energy of bulk flow may occur, in the case of unsteady emission, when different shells of matter moving with different Γ collide with each other and give rise to “internal shocks”, or, in the case of single impulsive emission, when the ultrarelativistic shell of matter decelerates as it sweeps up matter from the external medium, giving rise to an “external shock”. The multiple baryon shells in the case of unsteady emission from the central engine would collide and eventually merge into one shell, which pushing into the external medium will also give rise to an external shock. Electrons as well as protons can be accelerated to high energies through Fermi mechanism at the internal and external shocks. In the multiple shell scenario, the prompt GRB phase is thought to result from the synchrotron radiation

(and possibly also inverse-Compton scattering) of the electrons accelerated in the internal shocks while the afterglow phase results from the same process(es) occurring at the external shock. In the single shell scenario, on the other hand, there are no internal shocks, and both the prompt and afterglow phases result from processes at the external shock as it moves through the external medium. Although currently internal-external shock scenario is popular (see Ref. [25] and references therein), it has been argued [26] recently that the single impulsive external shock scenario can efficiently reproduce the observed properties of the prompt as well the afterglow phases of GRBs.

As mentioned in the previous section, a possible TeV component of GRB radiation is most likely to be of a different origin than the process that gives rise to the keV–MeV burst component. Mainly three processes have been suggested so far which can give rise to TeV photon emission from GRBs within the context of the fireball model of GRBs: (1) Synchrotron self-compton (SSC) process (see, e.g., [27]), i.e., the inverse Compton scattering of sufficiently high energy electrons on the ambient synchrotron photons within the source, the synchrotron photons being radiated by the same non-thermal electron population; (2) photo-pion production by ultrahigh energy protons within the source and the subsequent decay of the neutral pions to photons [28, 29, 30], and (3) synchrotron radiation by ultrahigh energy protons above 10^{20} eV in the magnetic field within the source [14, 15, 16, 17]. In general, the required high energy non-thermal electrons and protons can be accelerated either in the internal shocks or in the external shock, and the associated TeV photons can be emitted either in the burst phase or the afterglow phase. In the present paper, we shall consider the case of prompt TeV photon emission in coincidence with the burst phase.

Both photo-pion production and the proton-synchrotron processes are motivated by the suggestion [18] that GRBs may be the sources of the observed ultrahigh energy cosmic rays (UHECR) [31] whose spectrum extends beyond 10^{20} eV. In this scenario, UHECR particles are assumed to be protons accelerated within GRBs. Thus, in this scenario, while the synchrotron radiation of electrons produces the observed low energy (keV–MeV) component, a high energy (GeV–TeV) component could be produced by the ultrahigh energy proton component either through synchrotron or photo-pion processes.

If one assumes that the total energy density of the high energy GeV–TeV component photons within the source is significantly higher than that of the low energy “BATSE” photons, as seems to be the case for the TeV photon emitting GRBs claimed to have been detected so far, and if one further assumes that the energy density of the magnetic field within the source is roughly in equipartition with the total energy density, then it can be shown [12] that, for production of photons of observed energy

\sim TeV and above, the proton-synchrotron process dominates over the photo-pion process, both processes being due to the same underlying non-thermal proton content within the source. On the other hand, if the SSC process were to produce the high energy component with a significantly higher energy density content than that of the low energy component, both components in this case being due to the same underlying non-thermal electron content within the source, then the energy density in the magnetic field would have to be significantly less than its equipartition value [12], a condition that is at variance with models in which GRBs are sources of UHECR, which by and large require a magnetic field within GRB close to the equipartition limit [18].

In this paper, we shall work within the framework of GRBs as sources of the observed UHECR up to $\sim 10^{20}$ eV and, based on arguments mentioned above, as far as the question of production of a high energy photon component of GRBs is concerned, we shall limit ourselves in the rest of this paper specifically to the proton-synchrotron model.

The proton-synchrotron process may also play an important role in the internal energetics of GRBs. For example, it has been argued (see, e.g., [16, 17, 20, 32]) that, if the fundamental source of energy of the GRBs is indeed the kinetic energy of the ultrarelativistic bulk flow of matter as in the fireball model, then, at least initially, one would expect the total energy content in protons to be higher than that in electrons by a factor of $\sim m_p/m_e \sim 2000$, where m_p and m_e are proton and electron rest mass, respectively. Immediately after dissipation of the kinetic energy of the bulk flow through formation of internal and external shocks, the total energy content of protons would, therefore, be higher than that of electrons. Transfer of energy from the protons to electrons through coulomb interactions is not efficient [32]. Instead, as suggested by Totani [32], protons accelerated to energies above 10^{20} eV may first produce TeV energy synchrotron photons which, in collision with the sub-MeV photons within the source, may produce e^+e^- pairs through $\gamma\gamma \rightarrow e^+e^-$, thereby providing another channel through which energy can be transferred from the protons to electrons. If this process is very efficient in a GRB, then that GRB will not be a significant emitter of TeV photons. If on the other hand, the above pair production process is not very efficient, then the TeV photons would escape, resulting in strong TeV photon emission. The efficiency of the above pair production process for the TeV photons turns out to be a sensitive function of the initial bulk Lorentz factor Γ (see below). Thus, small fluctuations in Γ from burst to burst could give rise to wide variation of the TeV photon output from burst to burst even if the initial total energy input in all GRBs lies in a narrow range. Of course, the total energy output of a GRB in TeV photons will also depend on the shape of the accelerated protons'

spectrum: If the proton spectrum is sufficiently hard so that most of the total energy in the proton component lies at the highest energy end of the spectrum where the synchrotron emission process is efficient, and if the pair-production process for the resulting TeV synchrotron photons is inefficient, then the bulk of the energy in the proton component (which is initially higher than that in the electron component) will escape from the source in the form of TeV photons, which may naturally explain the significantly higher total energy in the TeV photon component compared to that in the sub-MeV component estimated for the TeV photon emitting GRBs claimed to have been detected so far.

Before going into quantitative discussions in the following sections, it is necessary to specify the relativistic reference frames used in the calculations below. There are three reference frames of interest: (1) The “Wind Rest Frame” (WRF), which is comoving with the average ultrarelativistic “wind” shell, (2) the “lab” frame, in which the ultrarelativistic outflow moves with the average Lorentz factor Γ , and (3) the “observer’s frame” based on Earth. Quantities referred to in these frames will be indicated by the superscripts “WRF”, “lab” and “ob”, respectively. The “ob” frame quantities differ from the corresponding “lab” frame quantities only due to the cosmological redshift of the GRB source. Throughout this paper, physical quantities without any superscript for the reference frame will be understood to be referring to the WRF, unless explicitly stated otherwise.

3 The Proton-Synchrotron Model of TeV Photon Production in GRBs

3.1 The magnetic field strength in the wind rest frame

We assume that there is a magnetic field (B) within the GRB environment, the strength of which is determined by the condition that the total energy density in the system is approximately equipartitioned between the magnetic field energy density, $B^2/8\pi$, and total particle-radiation energy density, U . Following Totani [16, 17, 20, 32] and Ref. [12] we assume that $U \sim U_p \sim (m_p/m_e)U_\gamma$, where U_γ is the energy density of the low energy BATSE photon component (assumed to arise mainly through electron synchrotron radiation), and U_p is the energy density in the form of protons. Note that all the above quantities refer to the WRF. We thus have

$$\frac{B^2}{8\pi} = \xi_B U_\gamma \frac{m_p}{m_e}, \quad (1)$$

where ξ_B is the equipartition factor assumed to be of order unity. For a GRB at a given redshift z , the WRF energy density U_γ on the right hand side of Eq. (1) can be

expressed in terms of the observed variability time scale of the burst, Δt^{ob} , and the observed luminosity, L_L^{ob} , in the low energy (keV–MeV) BATSE component inferred from the measured fluence and the known distance (redshift), in the following way:

$$L_L^{\text{ob}} = \frac{L_L}{(1+z)^2} = \frac{1}{(1+z)^2} 4\pi (r_d^{\text{lab}})^2 \Gamma^2 c U_\gamma, \quad (2)$$

where

$$r_d^{\text{lab}} = 2\Gamma^2 c \Delta t^{\text{ob}} / (1+z) \quad (3)$$

is the lab-frame value of the characteristic “dissipation radius” where the internal shocks are formed and from where most of the radiation is emitted. Note that r_d^{lab} is the value of the dissipation radius as inferred by the observer at Earth from the measured variability time scale after correcting for the time dilation due to expansion of the Universe.

Note also that L_L^{ob} as defined above is the effective 4π luminosity of the source assuming isotropic emission. If, instead, the source emits non-isotropically, for example, in a jet with opening solid angle Ω , then the actual luminosity would be a factor $(\Omega/4\pi)$ smaller than L_L^{ob} . The same applies to the luminosity in the high energy component, L_H , used later. Obviously, our final results for the number of events per unit area in a detector on Earth and the associated signal-to-noise ratios are independent of whether or not the emission is isotropic, provided, of course, in the case of jetty emission, the emission jet from the source under consideration points toward Earth. Below we shall use the effective 4π luminosity in all our calculations.

Using equations (1) – (3), we can write

$$B = 6.8 \times 10^3 \frac{\xi_B^{1/2} (L_{L,51}^{\text{ob}})^{1/2} (1+z)^2}{\Gamma_{300}^3 \left(\frac{\Delta t^{\text{ob}}}{\text{sec}} \right)} \text{ Gauss}, \quad (4)$$

where $\Gamma_{300} \equiv \Gamma/300$, and $L_{L,51}^{\text{ob}} \equiv L_L^{\text{ob}}/10^{51} \text{ erg s}^{-1}$.

3.2 Synchrotron photon spectrum

The synchrotron radiation photons emitted by protons of energy E_p in a magnetic field of strength B have the characteristic energy

$$E_\gamma = \frac{3}{2} \frac{e\hbar B E_p^2}{m_p^3 c^5} \langle \sin \alpha \rangle, \quad (5)$$

where e is the proton electric charge, and $\langle \sin \alpha \rangle = \pi/4$ is the average value of the sine of the pitch angle α of the proton. Using Eq. (4) for the magnetic field, we get the relation between the proton energy and its synchrotron photon energy in the WRF:

$$\frac{E_p}{\text{GeV}} = \kappa_1 \left(\frac{E_\gamma}{\text{GeV}} \right)^{1/2}, \quad (6)$$

where

$$\kappa_1 = 1.3 \times 10^8 \frac{\Gamma_{300}^{3/2} \left(\frac{\Delta t^{\text{ob}}}{\text{sec}} \right)^{1/2}}{\xi_B^{1/4} \left(L_{\text{L},51}^{\text{ob}} \right)^{1/4} (1+z)}. \quad (7)$$

Note that we can use the general relation

$$E^{\text{ob}} = \frac{\Gamma}{1+z} E \quad (8)$$

between energy in the observer's frame and that in WRF, to express Eq. (6) in terms of observed energies:

$$\frac{E_p^{\text{ob}}}{\text{GeV}} = \kappa_2 \left(\frac{E_\gamma^{\text{ob}}}{\text{GeV}} \right)^{1/2}, \quad (9)$$

where

$$\kappa_2 = 2.3 \times 10^9 \frac{\Gamma_{300}^2 \left(\frac{\Delta t^{\text{ob}}}{\text{sec}} \right)^{1/2}}{\xi_B^{1/4} \left(L_{\text{L},51}^{\text{ob}} \right)^{1/4} (1+z)^{3/2}}. \quad (10)$$

Note that $\kappa_2 = \left(\frac{\Gamma}{1+z} \right)^{1/2} \kappa_1$.

Now, let

$$\frac{dn_p}{dE_p} = A_p \left(\frac{E_p}{\text{GeV}} \right)^{-\alpha_p} \quad (11)$$

be the differential spectrum of the protons (number density of protons per unit energy) accelerated in the internal shocks. The differential spectrum, dn_γ/dE_γ , of the synchrotron photons radiated by these protons is then related to the proton spectrum as

$$f_{\text{ps}}(E_p) E_p \frac{dn_p}{dE_p} dE_p = E_\gamma \frac{dn_\gamma}{dE_\gamma} dE_\gamma, \quad (12)$$

where $f_{\text{ps}}(E_p)$ is the fraction of energy of a proton of energy E_p lost to synchrotron radiation, and E_p and E_γ are related through Eq. (6).

The fraction $f_{\text{ps}}(E_p)$ is just the fractional energy loss of the proton of energy E_p through synchrotron radiation during one expansion timescale of the wind, i.e.,

$$f_{\text{ps}}(E_p) = \frac{t_{\text{exp}}}{t_{\text{ps}}(E_p)}, \quad (13)$$

where

$$\frac{1}{t_{\text{ps}}(E_p)} \equiv \frac{1}{E_p} \left(\frac{dE}{dt} \right)_{\text{ps}}(E_p) \quad (14)$$

is the inverse of the synchrotron loss time scale, with

$$\left(\frac{dE}{dt} \right)_{\text{ps}}(E_p) \simeq c \frac{4}{9} \left(\frac{e^2}{m_p c^2} \right)^2 \left(\frac{E_p}{m_p c^2} \right)^2 B^2 \quad (15)$$

(assuming $E_p \gg m_p c^2$ and isotropic distribution of the pitch angles), and

$$t_{\text{exp}} \simeq \frac{1}{\Gamma} \frac{r_{\text{d}}^{\text{lab}}}{c} \quad (16)$$

is the expansion time scale of the wind, both time scales being measured in the WRF.

Since $t_{\text{ps}}(E_p) \propto E_p^{-1}$, we see that protons of energy above a “break” energy E_{pb} given by the condition

$$t_{\text{ps}}(E_p = E_{pb}) = t_{\text{exp}}, \quad (17)$$

will lose all their energy through synchrotron emission within one expansion time scale of the wind, thus giving

$$f_{\text{ps}}(E_p) = \begin{cases} \frac{E_p}{E_{pb}}, & \text{if } E_p < E_{pb}, \\ 1, & \text{if } E_p \geq E_{pb}. \end{cases} \quad (18)$$

Using equations (14), (15) and (4) we get

$$\frac{1}{t_{\text{ps}}(E_p)} = 1.03 \times 10^{-11} \frac{\xi_B (L_{\text{L},51}^{\text{ob}}) (1+z)^4}{\Gamma_{300}^6 \left(\frac{\Delta t^{\text{ob}}}{\text{sec}} \right)^2} \left(\frac{E_p}{\text{GeV}} \right) \text{sec}^{-1}, \quad (19)$$

which, together with equations (17), (16) and (3) gives

$$E_{pb} \simeq 1.6 \times 10^8 \frac{\Gamma_{300}^5 \left(\frac{\Delta t^{\text{ob}}}{\text{sec}} \right)}{(1+z)^3 \xi_B (L_{\text{L},51}^{\text{ob}})} \text{GeV}. \quad (20)$$

Equations (12), (11), (6), (7), (18) and (20) then give the synchrotron photon spectrum in the WRF:

$$\frac{dn_\gamma}{dE_\gamma} = \frac{1}{2} A_p \kappa_1^{-\alpha_p+2} \begin{cases} \left(\frac{E_{\gamma b}}{\text{GeV}} \right)^{-1/2} \left(\frac{E_\gamma}{\text{GeV}} \right)^{-\alpha_p/2-1/2} & \text{if } E_\gamma < E_{\gamma b}, \\ \left(\frac{E_\gamma}{\text{GeV}} \right)^{-\alpha_p/2-1} & \text{if } E_\gamma \geq E_{\gamma b}, \end{cases} \quad (21)$$

where

$$E_{\gamma b} \equiv \kappa_1^{-2} \left(\frac{E_{pb}}{\text{GeV}} \right)^2 \text{ GeV} \quad (22)$$

$$= 1.5 \frac{\Gamma_{300}^7 \left(\frac{\Delta t^{\text{ob}}}{\text{sec}} \right)}{\xi_B^{3/2} (L_{\text{L},51}^{\text{ob}})^{3/2} (1+z)^4} \text{ GeV}, \quad (23)$$

is the “break” energy above which the synchrotron differential photon spectrum steepens by a power-law index 0.5 relative to the spectrum below that energy.

The spectrum (21) cuts off above an energy $E_{\gamma,\text{max}}$ given by

$$E_{\gamma,\text{max}} = \kappa_1^{-2} \left(\frac{E_{p,\text{max}}}{\text{GeV}} \right)^2 \text{ GeV}, \quad (24)$$

where $E_{p,\text{max}}$ is the maximum energy of the protons accelerated in the internal shocks. The acceleration time scale is $t_{\text{acc}}(E_p) \sim 2\pi\eta r_L(E_p)/c$, where $r_L(E_p) = E_p/(eB)$ is the Larmor radius and η a factor of order unity. For reasonable ranges of values of the parameters of our interest, we have $t_{\text{acc}} < t_{\text{exp}} \leq t_{\text{ps}}$ for $E_p \leq E_{pb}$, $t_{\text{acc}} \leq t_{\text{ps}} < t_{\text{exp}}$ for $E_{pb} < E_p \leq E_{p,\text{max}}$, and $t_{\text{ps}} < t_{\text{acc}}$ for $E_p > E_{p,\text{max}}$. (Here the equality signs in the time scale conditions refer to the corresponding equality signs in the energy conditions.) Thus, $E_{p,\text{max}}$ is in general larger than E_{pb} , and is determined by synchrotron energy loss, i.e., by the condition

$$t_{\text{acc}}(E_{p,\text{max}}) \simeq t_{\text{ps}}(E_{p,\text{max}}), \quad (25)$$

Equation (25), together with equations (14), (15) and (4), gives

$$E_{p,\text{max}} = 9.8 \times 10^8 \eta^{-1/2} \frac{\Gamma_{300}^{3/2} \left(\frac{\Delta t^{\text{ob}}}{\text{sec}} \right)^{1/2}}{\xi_B^{1/4} (L_{\text{L},51}^{\text{ob}})^{1/4} (1+z)} \text{ GeV}, \quad (26)$$

and consequently,

$$E_{\gamma,\text{max}} = 54.73 \eta^{-1} \text{ GeV}. \quad (27)$$

In the observer's frame on Earth, equations (26), (27) and (8) give

$$E_{p,\max}^{\text{ob}} = 3 \times 10^{11} \eta^{-1/2} \frac{\Gamma_{300}^{5/2} \left(\frac{\Delta t^{\text{ob}}}{\text{sec}} \right)^{1/2}}{\xi_B^{1/4} \left(L_{\text{L},51}^{\text{ob}} \right)^{1/4} (1+z)^2} \text{GeV}, \quad (28)$$

and

$$E_{\gamma,\max}^{\text{ob}} = 1.64 \times 10^4 \eta^{-1} \left(\frac{\Gamma_{300}}{1+z} \right) \text{GeV}. \quad (29)$$

In the numerical calculations below, we shall take $\eta = 1$. Note that equation (28) shows that, depending on values of the various parameters involved, protons may in principle be accelerated to (observed) energies above 10^{20} eV in GRBs.

4 Optical Depth of High Energy Photons due to e^+e^- pair Production and the Spectrum of Photons at Source and at Earth

The spectrum, eq. (21), of the high energy photons produced by the proton synchrotron mechanism, has to be corrected for optical depth of the produced photons within the source (“internal optical depth”) in order to calculate the spectrum of the high energy photons emerging from the GRB source. The emergent spectrum so calculated has to be then further corrected for optical depth of the emitted high energy photons in the intergalactic medium (“external optical depth”) on their way from the source to Earth, in order to calculate the spectrum of photons arriving at Earth.

The dominant source of the optical depth of high energy photons within the GRB environment as well as in the intergalactic medium is e^+e^- pair production due to collision of the high energy photons with other photons in the medium. A test photon of energy E_t can produce an e^+e^- pair in a collision with a target photon of energy ϵ greater than a certain threshold value ϵ_{th} given by

$$\epsilon_{\text{th}} = \frac{2(m_e c^2)^2}{E_t(1 - \cos \theta)}, \quad (30)$$

where θ is the angle between the two photons' directions of propagation. The cross section for this process for target photon energies ϵ above the threshold is [33]

$$\sigma_{\gamma\gamma}(E_t, \epsilon, \theta) = \frac{3}{16} \sigma_T (1 - \beta^2) \left[(3 - \beta^4) \ln \frac{1 + \beta}{1 - \beta} - 2\beta(2 - \beta^2) \right], \quad (31)$$

where σ_T is the Thomson cross section and $\beta = [1 - (\epsilon_{\text{th}}/\epsilon)]^{1/2}$ is the center-of-mass speed of the outgoing pair particles in units of c .

4.1 Internal Optical Depth and the Lab Frame Spectrum of Photons Emerging from the Source

Let us first calculate the internal optical depth. The mean free path, $\ell_{\gamma\gamma}$, of the test photon of energy E_t within the GRB source can be written, in the WRF, assuming isotropic distribution of the photons in the WRF, as [34]

$$\ell_{\gamma\gamma}^{-1}(E_t) = \frac{1}{2} \int d(\cos \theta) (1 - \cos \theta) \int_{\epsilon_{\text{th}}(E_t, \cos \theta)}^{\infty} d\epsilon \frac{dn}{d\epsilon} \sigma_{\gamma\gamma}, \quad (32)$$

where $dn/d\epsilon$ is the differential number density of the target photons (in the WRF) within the GRB source.

From Eq. (30), we see that the lowest target photon threshold energy (which occurs for $\cos \theta = -1$) in the WRF, for a given test photon of observed energy $E_t^{\text{ob}} = (\Gamma/(1+z))E_t$, is

$$\epsilon_{\text{th}, \min} = 250 \left(\frac{300 \text{ GeV}}{E_t^{\text{ob}}} \right) \frac{\Gamma_{300}}{1+z} \text{ eV}, \quad (33)$$

which, in the observer's frame takes the form

$$\epsilon_{\text{th}, \min}^{\text{ob}} = 75 \left(\frac{300 \text{ GeV}}{E_t^{\text{ob}}} \right) \left(\frac{\Gamma_{300}}{1+z} \right)^2 \text{ keV}, \quad (34)$$

From the above two equations, it is clear that, for the high energy photons of our interest, the target photons for pair production within the GRB source are mainly those that have observed energies typically in the low (keV–MeV) energy BATSE range. We shall, therefore, assume that the dominant contribution to the internal optical depth due to pair production for the high energy photons of our interest comes from target photons that constitute the observed low energy BATSE photon component. With this assumption, then, we can write

$$\frac{dn}{d\epsilon} \propto \frac{d\phi^{\text{ob}}}{d\epsilon^{\text{ob}}}, \quad (35)$$

where $d\phi^{\text{ob}}/d\epsilon^{\text{ob}}$ is the differential spectrum of the observed BATSE photons, which, for most GRBs, is known to be well-fitted, within the BATSE energy range between $\epsilon_{\min}^{\text{ob}} \approx 20 \text{ keV}$ to $\epsilon_{\max}^{\text{ob}} \approx 2 \text{ MeV}$, by a power-law with a break [35],

$$\frac{d\phi^{\text{ob}}}{d\epsilon^{\text{ob}}} \propto \begin{cases} \left(\epsilon_b^{\text{ob}} \right)^{\beta_l - \beta_h} \left(\epsilon^{\text{ob}} \right)^{-\beta_l}, & \text{if } \epsilon^{\text{ob}} < \epsilon_b^{\text{ob}}, \\ \left(\epsilon^{\text{ob}} \right)^{-\beta_h}, & \text{if } \epsilon^{\text{ob}} \geq \epsilon_b^{\text{ob}}, \end{cases} \quad (36)$$

where $\epsilon_b^{\text{ob}} \approx 1 \text{ MeV}$ is the break energy of the observed spectrum, and $\beta_l \approx 1$ and $\beta_h \approx 2$.

The proportionality constant in (35) can be determined in terms of the observed luminosity L_L^{ob} defined in equation (2) through the condition

$$\int_{\epsilon_{\min}}^{\epsilon_{\max}} \epsilon \frac{dn}{d\epsilon} d\epsilon = U_\gamma = \frac{(1+z)^2 L_L^{\text{ob}}}{4\pi c (r_d^{\text{lab}})^2 \Gamma^2}, \quad (37)$$

together with the relation (8) between the energies in the WRF and observer's frame.

We can now perform the two integrals in equation (32) to calculate $\ell_{\gamma\gamma}^{-1}$. In doing this, it is convenient [34] to change variables from $(\epsilon, \cos \theta)$ to (ϵ, s) , with variable s defined as

$$s \equiv \frac{\epsilon E_t (1 - \cos \theta)}{2(m_e c^2)^2} = \frac{\epsilon}{\epsilon_{\text{th}}} \equiv s_0 z, \quad (38)$$

with

$$s_0 \equiv \frac{\epsilon E_t}{(m_e c^2)^2}, \quad z \equiv \frac{1}{2}(1 - \cos \theta). \quad (39)$$

Note that $\beta = (1 - 1/s)$, so $\sigma_{\gamma\gamma}$ now becomes a function of the single variable s , allowing us to write equation (32) as

$$\ell_{\gamma\gamma}^{-1}(E_t) = \frac{3}{8} \sigma_T \left(\frac{m_e^2 c^4}{E_t} \right)^2 \int_{\frac{m_e^2 c^4}{E_t}}^{\infty} d\epsilon \epsilon^{-2} \frac{dn}{d\epsilon} \varphi[s_0(\epsilon)], \quad (40)$$

where

$$\varphi[s_0(\epsilon)] = \int_1^{s_0(\epsilon)} s \tilde{\sigma}(s) ds, \quad \text{with } \tilde{\sigma}(s) \equiv \frac{16}{3} \frac{\sigma_{\gamma\gamma}}{\sigma_T}. \quad (41)$$

The ϵ and s integrals are now decoupled and are easily evaluated numerically. Finally, the internal optical depth $\tau_{\text{int}}(E_t)$ for the high energy test photon of energy E_t is given by the ratio of the wind expansion time scale $t_{\text{exp}} = r_d^{\text{lab}}/c\Gamma$ and the mean two-photon collision time scale $t_{\gamma\gamma} = \ell_{\gamma\gamma}/c$, giving

$$\tau_{\text{int}}(E_t) = \frac{r_d^{\text{lab}}}{\Gamma} \ell_{\gamma\gamma}^{-1}. \quad (42)$$

The dependence of τ_{int} on E_t and on various other parameters in the problem can be easily extracted if we make the simplifying approximation $\sigma_{\gamma\gamma} \simeq (3/16)\sigma_T = \text{constant}$ ³. With this approximation, $\tilde{\sigma}(s) = 1$, and $\varphi[s_0(\epsilon)] = (s_0^2 - 1)/2$, so the ϵ integral in equation (40) can be performed analytically with the power-law form of

³Actually, for $s \gg 1$, $\sigma_{\gamma\gamma} \propto (\ln s)/s$, but the spectrum of target photons falls off rapidly for $\epsilon > \epsilon_{\text{th}}$, so this approximation does not introduce large error.

$dn/d\epsilon$ given by equations (35), (36) and (37). For $\beta_l = 1$, $\beta_h = 2$, we get (in terms of quantities measured in the observer's frame)

$$\tau_{\text{int}}(E_t^{\text{ob}}) \simeq \frac{3\sigma_T L_L^{\text{ob}} \mathcal{C}}{64\pi c^2 \Delta t^{\text{ob}}} \begin{cases} \frac{(1+z)^4}{\Gamma^6} \frac{1}{3} \frac{E_t^{\text{ob}}}{m_e^2 c^4}, & \text{for } E_t^{\text{ob}} < E_{t,s}^{\text{ob}}, \\ \frac{(1+z)^2}{\Gamma^4} \left[\frac{1}{4\epsilon_b^{\text{ob}}} + \frac{1}{12\epsilon_b^{\text{ob}}} \left(\frac{E_{t,s}^{\text{ob}}}{E_t^{\text{ob}}} \right)^2 + \frac{1}{2\epsilon_b^{\text{ob}}} \ln \frac{E_t^{\text{ob}}}{E_{t,s}^{\text{ob}}} \right], & \text{for } E_t^{\text{ob}} \geq E_{t,s}^{\text{ob}}, \end{cases} \quad (43)$$

where

$$\mathcal{C} = \frac{1}{\left(\frac{\epsilon_b^{\text{ob}} - \epsilon_{\text{min}}^{\text{ob}}}{\epsilon_b^{\text{ob}}} \right) + \ln \left(\frac{\epsilon_{\text{max}}^{\text{ob}}}{\epsilon_b^{\text{ob}}} \right)}, \quad (44)$$

and

$$E_{t,s}^{\text{ob}} = \left(\frac{\Gamma}{1+z} \right)^2 \frac{m_e^2 c^4}{\epsilon_b^{\text{ob}}} = 22.5 \left(\frac{\Gamma_{300}}{1+z} \right)^2 \left(\frac{1 \text{ MeV}}{\epsilon_b^{\text{ob}}} \right) \text{ GeV}, \quad (45)$$

is the energy below which, as equation (43) shows, $\tau_{\text{int}} \propto E_t^{\text{ob}}$, while $\tau_{\text{int}}(E_t)$ “saturates” to a roughly constant value above this energy with two E_t^{ob} dependent correction terms one of which falls off as $(E_t^{\text{ob}})^{-2}$ while the other increases with E_t^{ob} only as $\ln E_t^{\text{ob}}$.

Equation (43) also shows the sensitive dependence of τ_{int} on Γ . The results of our full numerical calculations of τ_{int} shown in Figures 1–4 clearly exhibit the expected dependence of τ_{int} on various parameters in the problem.

With the internal optical depth calculated as above, the total number of high energy photons emitted by the GRB per unit time per unit energy as measured in the lab frame is given by

$$\frac{dN_\gamma^{\text{lab}}}{dE_\gamma^{\text{lab}} dt^{\text{lab}}} = 4\pi \left(r_d^{\text{lab}} \right)^2 c \frac{dn_\gamma}{dE_\gamma} \exp(-\tau_{\text{int}}(E_\gamma)), \quad (46)$$

where dn_γ/dE_γ is as given by equation (21), and with $E_\gamma = E_\gamma^{\text{lab}}/\Gamma$. The total photon luminosity in the high energy component emitted by the GRB source (due to proton synchrotron radiation), as measured by a lab frame observer, is

$$L_H^{\text{lab}} \equiv \int E_\gamma^{\text{lab}} \frac{dN_\gamma^{\text{lab}}}{dE_\gamma^{\text{lab}} dt^{\text{lab}}} dE_\gamma^{\text{lab}} = 4\pi \left(r_d^{\text{lab}} \right)^2 \Gamma^2 c \int_{E_{\gamma,\text{min}}}^{E_{\gamma,\text{max}}} E_\gamma \frac{dn_\gamma}{dE_\gamma} \exp(-\tau_{\text{int}}(E_\gamma)) dE_\gamma, \quad (47)$$

where $E_{\gamma,\text{max}}$ is given by equation (27). The exact value of $E_{\gamma,\text{min}}$ is not important as long as we take $E_{\gamma,\text{min}} < E_{\gamma b}$ since, the power-law index of the spectrum (21)

being less than 2 (for $\alpha_p < 3$ which we always assume to be the case), the dominant contribution to the energy integral in the region $E_{\gamma,\min} < E_\gamma \leq E_{\gamma b}$ comes from its value at $E_{\gamma b}$. We use equation (47) to eliminate the constant A_p appearing in equations (11) and (21) in terms of L_H^{lab} which we shall take as a free parameter. This completely fixes the lab frame emission spectrum of the high energy component given by equation (46).

4.2 External Optical Depth and the Spectrum of High Energy Photons at Earth

Due to expansion of the Universe, the energies of individual photons are decreased by a factor of $(1+z)$ and time intervals are stretched by a factor of $(1+z)$, where z is the redshift of the GRB source. Therefore, the spectrum of photons arriving at Earth (giving number of photons striking the top of the atmosphere per unit area per unit energy per unit time) is simply given by

$$\frac{dN_\gamma^{\text{ob}}}{dAdE_\gamma^{\text{ob}}dt^{\text{ob}}}(E_\gamma^{\text{ob}}) = \frac{1}{4\pi D_z^2} \frac{dN_\gamma^{\text{lab}}}{dE_\gamma^{\text{lab}}dt^{\text{lab}}}(E_\gamma^{\text{lab}}) \exp\left(-\tau_{\text{ext}}(E_\gamma^{\text{lab}})\right), \quad (48)$$

where, on the right hand side, $E_\gamma^{\text{lab}} = (1+z)E_\gamma^{\text{ob}}$, $\tau_{\text{ext}}(E_\gamma^{\text{lab}})$ is the external optical depth, due to pair production through two-photon collision in the intergalactic medium, of a photon originating with energy E_γ^{lab} at the source, and D_z is the radial coordinate distance of the GRB source at redshift z .

For a spatially flat Universe (which we shall assume to be the case) with $\Omega_\Lambda + \Omega_m = 1$, where Ω_Λ and Ω_m are, respectively, the contribution of the cosmological constant and matter to the energy density of the Universe in units of the critical energy density, $3H_0^2/8\pi G$, the radial coordinate distance D_z is given by [36]

$$D_z = \left(\frac{c}{H_0}\right) \int_0^z \frac{dz'}{\sqrt{\Omega_\Lambda + \Omega_m(1+z')^3}}. \quad (49)$$

Here H_0 is the Hubble constant in the present epoch. In our calculations, we shall use the currently popular values $\Omega_\Lambda = 0.7$, $\Omega_m = 0.3$, and $H_0 = 65 \text{ km sec}^{-1} \text{ Mpc}^{-1}$.

The main contribution to the external optical depth τ_{ext} of GeV–TeV photons comes from e^+e^- pair production due to collisions with the photons constituting the intergalactic infrared background, and has been studied by a number of authors. We shall use the optical depths given in [13], where a parametrization has been given for $\tau(E_\gamma, z)$ for small z appropriate for our purpose. In our numerical calculations we use the optical depths given in Ref. [13] for the higher level of intergalactic infrared

background in order to have conservative estimate of the number of muons produced in the detector.

5 TeV Photon Signal from GRBs in a ICECUBE Class Detector

Photons of sufficiently high energy striking the earth's atmosphere interact with the air nuclei to produce pions; these photo-pions are the major source of muon production by photons in atmospheric air-showers, among other possible physical processes like direct pair production of muons by photons or photo-produced charm decays. As first suggested by AH [24], it may be possible to detect the TeV photons from GRBs by detecting these (downward-going) muons created by the TeV photons in the Earth's atmosphere in AMANDA/ICECUBE detectors. Our aim in this paper is to explore this possibility within the context of a specific model of TeV gamma ray production in GRBs discussed in the previous sections.

5.1 Muons in photon-induced air-showers and muon signal-to-noise ratio

The number of muons with energy above E_μ in an air-shower produced by a single photon of energy E_γ^{ob} striking the top of the atmosphere can be parametrized [37, 24], for E_μ in the range 100 GeV to 1 TeV, by the formula

$$N_\mu(E_\gamma^{\text{ob}}, \geq E_\mu) \simeq \frac{2.14 \times 10^{-5}}{\cos \theta} \frac{1}{(E_\mu / \cos \theta)} \frac{E_\gamma^{\text{ob}}}{(E_\mu / \cos \theta)}, \quad (50)$$

where θ is the zenith angle of the photon source, and all energies are in TeV units. The above parametrization is valid for $E_\gamma^{\text{ob}}/E_\mu \geq 10$ [24].

The total number of muons with energy in excess of a threshold muon energy, $E_{\mu,\text{th}}$, in a detector of effective area A_{eff} due to a single GRB of redshift z and observed duration T^{ob} can then be written as

$$N_\mu(\geq E_{\mu,\text{th}}) = A_{\text{eff}} T^{\text{ob}} \int_{E_{\gamma,\text{th}}^{\text{ob}}}^{E_{\gamma,\text{max}}^{\text{ob}}} dE_\gamma^{\text{ob}} \frac{dN_\gamma^{\text{ob}}}{dA dE_\gamma^{\text{ob}} dt^{\text{ob}}} N_\mu(E_\gamma^{\text{ob}}, \geq E_{\mu,\text{th}}), \quad (51)$$

where $E_{\gamma,\text{th}}^{\text{ob}} \simeq 10 \times E_{\mu,\text{th}}/\cos \theta$ is the minimum photon energy needed to produce muons of energy $E_{\mu,\text{th}}$ in the atmosphere [24], θ being the zenith angle of the photon source.

Equation (51) constitutes our signal, $S = N_\mu(\geq E_{\mu,\text{th}})$. This must then be compared to the background of atmospheric muons created by cosmic rays in the Earth's atmosphere. The differential spectrum of cosmic ray produced muons is given by [38]

$$\frac{dN_{\mu,\text{B}}}{dAdtd\Omega dE_\mu} \approx \frac{0.14E_\mu^{-2.7}}{\text{cm}^2 \text{ s sr GeV}} \left\{ \frac{1}{1 + \left(\frac{1.1E_\mu \cos \theta}{115 \text{ GeV}}\right)} + \frac{0.054}{1 + \left(\frac{1.1E_\mu \cos \theta}{850 \text{ GeV}}\right)} \right\}. \quad (52)$$

The number of background muons in the detector is, therefore,

$$B \equiv N_{\mu,\text{B}}(\geq E_{\mu,\text{th}}) = A_{\text{eff}} T^{\text{ob}} \Delta\Omega \int_{E_{\mu,\text{th}}}^{\infty} \frac{dN_{\mu,\text{B}}}{dAdtd\Omega dE_\mu} dE_\mu, \quad (53)$$

where we have included in the background the contribution only from the observed duration of the burst and from within a solid angle $\Delta\Omega = (\pi\delta\theta/180)^2$ around the direction of the burst, $\delta\theta$ being the angular resolution (in degrees) of the detector. For AMANDA/ICECUBE type detector, $\delta\theta$ is typically a few degrees. We then define the signal-to-ratio, S/N , as

$$\frac{S}{N} \equiv \frac{S - B}{\sqrt{B}}. \quad (54)$$

5.2 Muon threshold energy and effective area of detector for downward-going muons

For a muon to be detected by ICECUBE, it must have an energy $\gtrsim 100 \text{ GeV}$ [21] within the detector volume. However, unlike in the case of the neutrino-induced muons which can be created by the neutrinos within or near the detector volume, the gamma ray induced muons in the atmosphere will have to have sufficient energy at the surface to reach the detector volume deep within ice (at a depth of $\gtrsim 1 \text{ km}$) and still have enough energy left to satisfy the trigger for the detector. This requires [39], for ICECUBE, a threshold muon energy of $E_{\mu,\text{th}} \gtrsim 250 \text{ GeV}$ at the surface for a vertical muon. In this paper we take $E_{\mu,\text{th}} = 250 \text{ GeV}$ in our numerical calculations of the muon signal-to-noise ratio for ICECUBE.

We also need to specify what value to take for the effective area of the AMANDA/ICECUBE detectors for downward-going muons. As is well-known, these detectors are primarily designed to detect the upward-going muons created in the antarctic ice sheet by upward-going neutrinos from astrophysical sources, the main source of background for which is the upward-going muons due to upward-going atmospheric neutrinos. Most of the PMTs constituting the optical modules (OMs) are, therefore, placed downward-facing, while only a small number of PMTs are kept upward-facing. The AMANDA-B10 detector [40], for example, has a total of 302

OMs, in 295 of which the PMTs are downward-facing, while 7 OMs have upward-facing PMTs. However, because of scattering of light in the ice surrounding the OMs, the OMs are not completely blind to light from its backward hemisphere. This effect makes each OM a relatively more isotropic light sensor in ice than in vacuum. For AMANDA-B10 detector, Ref. [40] estimates the effective relative sensitivity of an OM to be $\sim 67\%$ in the forward hemisphere and $\sim 33\%$ in the backward hemisphere. From this, we can estimate that the effective area of the AMANDA-B10 detector for downward-going muons would be $\sim 1/2$ of that for upward-going muons.

The above discussion only serves to illustrate that although underice muon detectors like AMANDA/ICECUBE are designed to optimally detect the upward-going muons, the effective area of the detector for downward-going muons is still a significant fraction of its effective area for upward-going muons.

Of course, the effective area for muon detection depends on the energy of the muon and also on the zenith angle (θ) of the muon's direction of propagation. Figure 23 of Ref. [40] shows that for the AMANDA-B10 detector, the effective area for upward-going ($\cos\theta \approx -1$) muons is $\approx 9000\text{m}^2$ for muons in the energy range 100 – 1000 GeV. The effective area then decreases with increasing $\cos\theta$ reaching a small value at $\cos\theta = 0$ (horizontal direction). However, following the discussion in the previous paragraph, we expect that the effective area will increase again as we go above the horizon, i.e., as $\cos\theta$ increases from 0 toward 1 (directly downward-going), with the value of effective area roughly $1/2$ of the corresponding value at the corresponding angle below the horizon.

As will be clear from our results discussed in the next section, the effective area for AMANDA-B10, and for that matter even the AMANDA-II detector, is not large enough to detect the TeV photon signal from GRBs with any reasonable degree of confidence within the context of the proton-synchrotron model discussed above, unless the GRB is extraordinarily bright in TeV photons. We shall, therefore, consider their detectability in the proposed ICECUBE detector which may reach an effective area of $\sim 10^6\text{m}^2$ for upward-going muons (at $\cos\theta = -1$). For the purpose of illustrating the kind of numbers for the signal-to-noise ratio we may expect in a ICECUBE class detector, we may assume that the ratio of the effective area for down-going muons to that for upward-going muons in ICECUBE will be roughly similar to that in the AMANDA-B10. We shall, therefore, take a value of $\sim 5 \times 10^5\text{m}^2$ as a fiducial value of the effective area for directly downward-going muons in ICECUBE for the muon energy range of our interest. Our results for the signal-to-noise ratio discussed in the next section can be easily scaled (as $\sqrt{A_{\text{eff}}}$) for the actual effective area.

6 Results and Discussions

We now discuss our main results. There are 11 free parameters in the model. These are: $L_{L,51}^{\text{ob}}$, ξ_B , β_l , β_h , ϵ_b^{ob} , Δt^{ob} , T^{ob} , Γ , z , L_H^{lab} , and α_p . Out of these we fix $L_{L,51}^{\text{ob}} = 1$, $\xi_B = 0.5$, $\beta_l = 1$, $\Delta t^{\text{ob}} = 0.5 \text{ sec}$, and $T^{\text{ob}} = (1+z)10 \text{ sec}$, and study the dependence of our various results on the other remaining free parameters. Scalings of our results with respect to the fixed parameters are obvious from the relevant equations given in the earlier sections.

Figures 1–4 show how the internal optical depth due to pair production within the GRB source as a function of the observed energy depends on various parameters that characterize the burst. The functional dependence on energy is as expected from the approximate analytic expression for τ_{in} given by equation (43), i.e., τ_{in} increases with energy up to a saturation energy given by equation (45) beyond which τ_{in} is approximately constant.

The most sensitive dependence of τ_{in} is on Γ as indicated by equation (43) and as shown in Fig. 1: Larger values of Γ give smaller values of τ_{in} , and thus depending on a moderately large value of Γ in the range, say, 300–500, we can have $\tau_{\text{in}} \lesssim 1$.

Fig. 2 shows how $\tau_{\text{in}}(E_\gamma^{\text{ob}})$ depends on redshift of the burst. For a given value of the L_L^{ob} , higher redshift implies higher luminosity at the source. This in turn implies higher density of target photons for pair production inside the source, giving higher internal optical depth. Also, clearly, τ_{in} depends on the spectrum of the target photons within the source. We show the dependence of $\tau_{\text{in}}(E_\gamma^{\text{ob}})$ on two of the parameters that determine the target photon spectrum, namely, the break energy ϵ_b^{ob} (Fig. 3) and the power-law index β_h of the spectrum beyond the break (Fig. 4).

In Fig. 5 we display for illustration a typical predicted spectrum of the high energy component of a GRB due to proton-synchrotron process, where we also show the observed low energy “BATSE” spectrum for comparison. The effects of the internal and intergalactic optical depths due to pair production on the spectrum of the high energy component are also shown.

In Figures 6–8 we show how the signal-to-noise ratio in the detector depends on various parameters that characterize the burst. In all these figures, as also in Fig. 9, we assume an effective area of the detector for downward-going muons to be $\sim 5 \times 10^5 \text{ m}^2$, assume the source to be at zero zenith angle, and take the threshold muon energy (at the surface) for detection by ICECUBE to be 250 GeV. Figure 6 shows the dependence of the signal-to-noise ratio on the redshift of the GRB for three different values of the emitted luminosity in the high energy component at the source, L_H^{lab} . Note that L_H^{lab} , as defined in equation (47), is the effective 4π luminosity including the correction due

to internal optical depth. It is clear that for reasonable values of other parameters, detectability of the high energy component for GRBs at redshifts beyond about 0.05 requires excessively high values of $L_{\text{H}}^{\text{lab}}$ upward of $\sim 10^{58}$ ergs/sec. Dependence of the signal-to-noise ratio on the Lorentz factor Γ of the underlying fireball model of the GRB is shown in Fig. 7. From Fig. 7, we see that TeV photons from a GRB at redshift $z \sim 0.1$ is detectable with a signal-to-noise ratio of ~ 10 if $L_{\text{H}}^{\text{lab}} \sim 5 \times 10^{57}$ ergs/sec and $\Gamma \simeq 400$.

In the proton-synchrotron model under consideration, the high energy photon spectrum depends on the spectrum of the protons accelerated within the source. In Fig. 8, we show the dependence of the signal-to-noise ratio on the power-law index (α_p) of the differential spectrum of the protons, for various values of the redshift of the GRB. As expected, a steeper proton spectrum (i.e., larger values of α_p) gives a steeper synchrotron photon spectrum, which gives smaller number of high energy photons emitted from the source and hence smaller signal-to-ratio in the detector. This dependence on α_p is summarized in Fig. 9 where we show the behavior of the minimum luminosity in the high energy component, $L_{\text{H}}^{\text{lab}}$, required for detection with a signal to noise ratio of 5 or larger, as a function of α_p , for various values of the redshift z of the GRB. Clearly, as expected, a harder proton spectrum (i.e., smaller values of α_p) gives better prospect for detectability of the TeV photons in the proton-synchrotron model.

From the above discussions while it is clear that, within the context of the proton synchrotron model, the energetic requirement for detectability of a possible high energy (\gtrsim TeV) photon component of GRBs in ICECUBE class detector is admittedly rather high, the required total energy estimates are not implausible, especially for reasonably close-by GRBs at redshifts < 0.05 or so, as seen from Fig. 9.

We may compare the luminosity requirements discussed above for TeV photons with that for ultrahigh energy protons in the scenario where GRBs are sources of UHECR [18]. In order to explain the observed flux of UHECR, one needs a typical GRB to emit a total energy of $\sim \text{few} \times 10^{53}$ erg in UHE protons with energy $> 10^{19}$ eV, assuming that GRB rate evolves with redshift like the star formation rate in the Universe, with a local ($z = 0$) GRB rate of $\sim 5 \times 10^{-10} \text{ Mpc}^{-3} \text{ yr}^{-1}$ [41]. Note that the above number for the total energy in UHE protons refers to the total energy *escaping* from the GRB source in the form of UHE protons. The total energy in the UHE proton component produced *within* the GRB may be significantly higher, depending on the various energy loss processes of the UHE protons within the GRB source. If synchrotron radiation is the dominant energy loss process for the UHE protons within the GRB source, and if this process is very efficient, and further if the pair-production optical depth of the resulting GeV–TeV photons within the source is

sufficiently small, then the escaping GeV–TeV photon luminosity of the source may even be larger than the escaping UHE proton luminosity.

An indicator of the efficiency of the proton-synchrotron process is the value of the energy E_{pb} , given by equation (20), above which all protons lose all their energy through synchrotron radiation. Thus, smaller the value of this energy, higher is the synchrotron photon yield for a given spectrum of the protons. Specifically, if we assume that the internal pair-production optical depth of the high energy photons is negligible, then for a proton spectrum with index $\alpha_p = 2$, it is easy to show that the condition that the escaping high energy photon luminosity (due to synchrotron radiation of protons) be higher than the escaping proton luminosity is

$$E_{pb} < 2.72 (E_{p,\min} E_{p,\max})^{1/2}, \quad (55)$$

where $E_{p,\min}$ and $E_{p,\max}$ are the minimum and maximum energies of the protons, respectively. For appropriate choice of various parameters characterizing a GRB such as ξ_B (measuring the internal magnetic field), Γ and so on, the above condition may well be satisfied.

Lastly, we remind the reader that throughout the above discussion, the luminosity values we discussed refer to the isotropic effective 4π luminosities; as already mentioned, for collimated emission the required luminosity values would be appropriately smaller by a factor of $\Omega/4\pi$, where Ω is the solid angle of the collimated jet.

7 Summary and Conclusions

It is possible that GRBs emit not only sub-MeV photons as detected in satellite-borne detectors, but also higher energy photons extending to TeV energies. For a GRB photon spectrum falling with energy, as is usually the case, the non-detection of TeV photons in satellite-borne detectors could be due to their limited size. However, as first suggested in Refs. [23, 24], TeV photons from GRBs might be detectable in the existing under-ice muon detectors such as AMANDA and future detectors such as the proposed ICECUBE, by detecting the muons in the atmospheric showers created by TeV photons. In this paper, we have made detailed calculations of the detectability of possible TeV photons from individual GRBs by AMANDA/ICECUBE detectors within the context of a specific model of such high energy gamma ray production within GRBs, namely, the proton-synchrotron model, which requires protons to be accelerated to ultrahigh energies $\gtrsim 10^{20}$ eV within GRBs. In this model, the high energy component is distinct from, but may well be emitted in coincidence with, the usual “low” (keV–MeV) energy component observed by satellite-borne detectors. We have calculated the expected number of muons and the signal to noise ratio in these

detectors due to TeV gamma-rays from individual GRBs for various assumptions on their luminosity, distance (redshift), Lorentz Gamma factor of the underlying fireball model, and various spectral characteristics of the GRBs, including the effect of the absorption of TeV photons within the GRB as well as in the intergalactic infrared radiation background. The intergalactic absorption of TeV photons essentially precludes detection of TeV photons in the currently operating AMANDA detector for any reasonable values of the luminosity in the high energy component, but they may well be detectable in the proposed ICECUBE detector which may have an effective area for downward-going muons a factor of 100 larger than that in AMANDA. However, even in ICECUBE, only relatively close-by GRBs at redshifts < 0.05 or so can be expected to be detectable with any reasonable degree of confidence. The required isotropic luminosity of the high energy photon component is upward of 10^{56} ergs/sec and are generally found to be more than 3–4 orders of magnitude higher than typical estimated isotropic luminosities in the keV–MeV BATSE energy band. Such high luminosities may not, however, be impossible in some GRBs depending on various parameters that characterize the GRB.

8 Acknowledgment

One of us (NG) wishes to thank IIA, Bangalore for hospitality where a major part of this work was done. PB acknowledges partial support under the NSF US-India cooperative research grant # INT-9714627.

References

- [1] G.J. Fishman and C.A. Meegan, *Ann. Rev. Astron. Astrophys.* **33** (1995) 415.
- [2] J. van Paradijs, C. Kouveliotou and R. A. M. J. Wijers, *Ann. Rev. Astron. Astrophys.* **38** (2000) 379.
- [3] J.E. Rhoads, *Astrophys. J.* **525** (1999) 737.
- [4] D.A. Frail et al., *Astrophys. J.* **562** (2001) L55.
- [5] E.J. Schneid et al, *Astron. Astrophys.* **255** (1992) L13.
- [6] K. Hurley et al, *Nature* **372** (1994) 652.
- [7] J.R. Catelli, B.L. Dingus and E.J. Schneid, in *Gamma Ray Bursts*, ed. C. A. Meegan (New York, AIP, 1997).
- [8] M. Amenomori et al, *Astron. Astrophys.* **311** (1996) 919.
- [9] L. Padilla et al, *Astron. Astrophys.* **337** (1998) 43.
- [10] R. Atkins et al, *Astrophys. J.* **533** (2000) L119; also see URL http://www.lanl.gov/milagro/the_milagro_collaboration.html.
- [11] J. Poirier et al, astro-ph/0004379.
- [12] P.C. Fragile, G.J. Mathews, J. Poirier and T. Totani, astro-ph/0206383.
- [13] F. W. Stecker and O. C. de Jager, *Astron. Astrophys.* **334** (1998) L85.
- [14] M. Vietri, *Phys. Rev. Lett.* **78** (1997) 4328.
- [15] M. Böttcher and C.D. Dermer, *Astrophys. J.* **499** (1998) L131.
- [16] T. Totani, *Astrophys. J* **509** (1998) L81.
- [17] T. Totani, *Astrophys. J.* **536** (2000) L23.
- [18] E. Waxman, *Phys. Rev. Lett.* **75** (1995) 386; M. Vietri, *Astrophys. J.* **453** (1995) 883.
- [19] R. A. Vazquez, astro-ph/9810231.
- [20] T. Totani, *Astropart. Phys.* **11** (1999) 451.

- [21] The ICECUBE proposal: see URL <http://pheno.physics.wisc.edu/icecube/>.
- [22] F. Halzen (for AMANDA Collaboration) Nucl. Phys. Proc. Suppl. **77** (1999) 474; E. Andres et al (AMANDA collaboration), Astropart. Phys. **13** (2000) 1.
- [23] F. Halzen, T. Stanev, and G. Yodh, Phys. Rev. D **55** (1997) 4475.
- [24] J. Alvarez-Muñiz and F. Halzen, Astrophys. J. **521** (1999) 928.
- [25] T. Piran, Phys. Rep. **314** (1999) 575; **333** (2000) 529.
- [26] C.D. Dermer and K.E. Mitman, astro-ph/0301340.
- [27] C.D. Dermer, J. Chiang, and K.E. Mitman, Astrophys. J. **537** (2000) 785.
- [28] E. Waxman and J. Bahcall, Phys. Rev. Lett. **78** (1997) 2292.
- [29] J.P. Rachen and P. Mészáros, Phys. Rev. D **58** (1998) 123005.
- [30] A. Mücke, J.P. Rachen, R. Engel, R. J. Protheroe, and T. Stanev, in *Proc. 19th Texas Symp. on Relativistic Astrophysics and Cosmology*, Paris, December 1998 (astro-ph/9905153).
- [31] For reviews, see, e.g., M. Nagano and A. A. Watson, Rev. Mod. Phys. **72** (2000) 689; P. Bhattacharjee and G. Sigl, Phys. Rep. **327** (2000) 109; A. Olinto, Phys. Rep. **333** (2000) 329.
- [32] T. Totani, Mon. Not. R. Astron. Soc. **307** (1999) L41.
- [33] See, e.g., V.B. Berestetskii, E.M. Lifshitz and L. P. Pitaevskii, *Quantum Electrodynamics* (New York: Pergamon, 1982), p. 371.
- [34] R.J. Gould and G.P. Schreder, Phys. Rev. **155** (1967) 1404.
- [35] D. Band et al, Astrophys. J **413** (1993) 281.
- [36] C.W. Misner, K.S. Thorne and J.A. Wheeler, *Gravitation* (W. H. Freeman, San Francisco, 1973).
- [37] F. Halzen, K. Hikasa and T. Stanev, Phys. Rev. D **34** (1986) 2061.
- [38] T.K. Gaisser, *Cosmic Rays and Particle Physics* (Cambridge Univ. Press, Cambridge, 1990), p. 71.
- [39] We thank the anonymous referee for pointing this out.

- [40] J. Ahrens et al (AMANDA Collaboration), Phys. Rev. **D66** (2002) 012005.
- [41] See, e.g., E. Waxman, in *Physics and Astrophysics of Ultra-High-Energy Cosmic Rays*, eds.: M. Lemoine and G. Sigl (Springer, Berlin, 2001), p. 122–154; J. N. Bahcall and E. Waxman, Phys. Lett. **B556** (2003) 1 (hep-ph/0206217 v5).

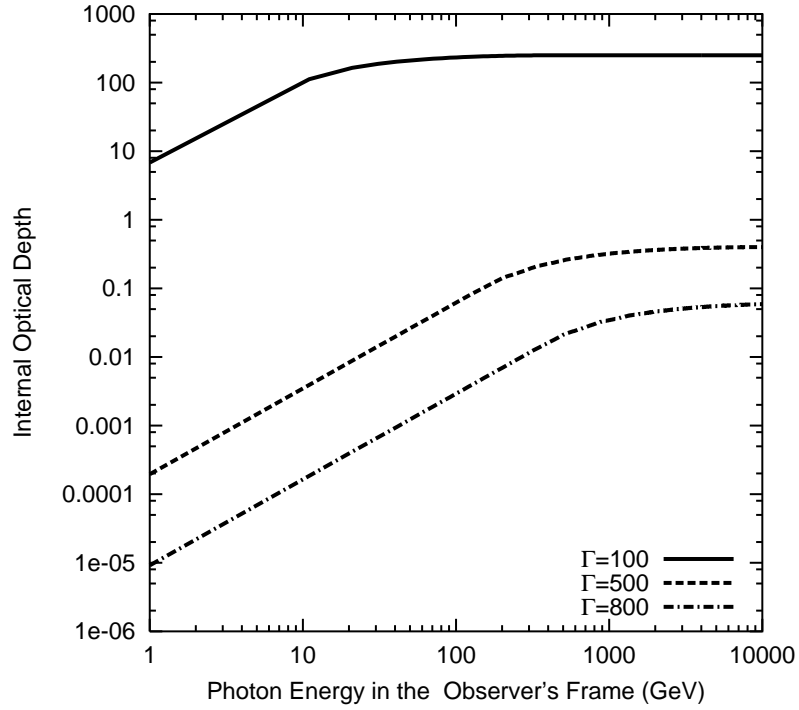


Figure 1: Internal optical depth as a function of the photon's energy in the observer's frame, for various values of Γ as indicated. Values taken for other relevant parameters are: $L_{L,51}^{\text{ob}} = 1$, $\beta_l = 1$, $\beta_h = 2.25$, $\epsilon_b^{\text{ob}} = 0.5$ MeV, $\Delta t^{\text{ob}} = 0.5$ sec, and $z = 0.1$.

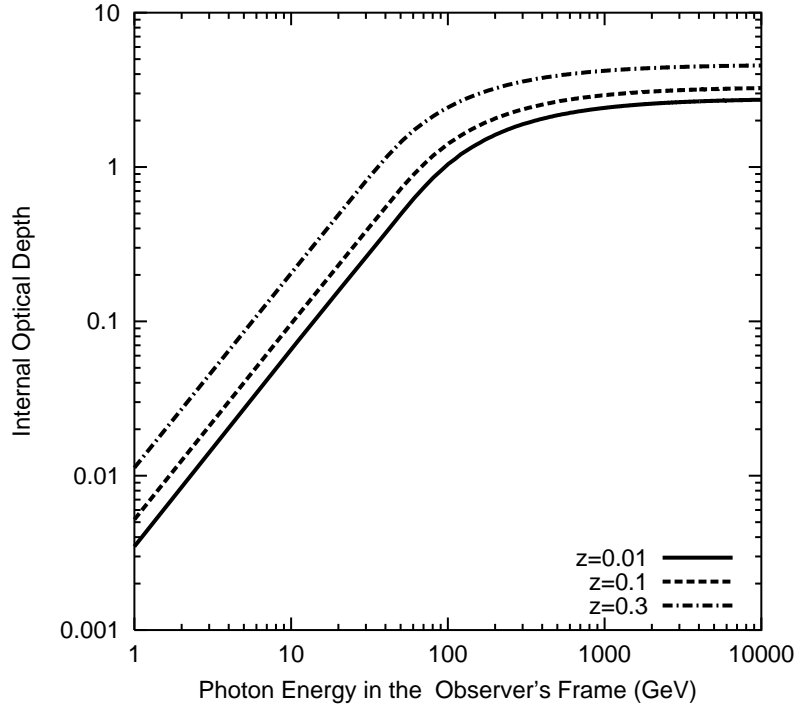


Figure 2: Internal optical depth as a function of the photon's energy in the observer's frame, for various values of the redshift z of the GRB as indicated. Values taken for other relevant parameters are: $L_{L,51}^{\text{ob}} = 1$, $\beta_l = 1$, $\beta_h = 2.25$, $\epsilon_b^{\text{ob}} = 0.5 \text{ MeV}$, $\Delta t^{\text{ob}} = 0.5 \text{ sec}$, and $\Gamma = 300$.

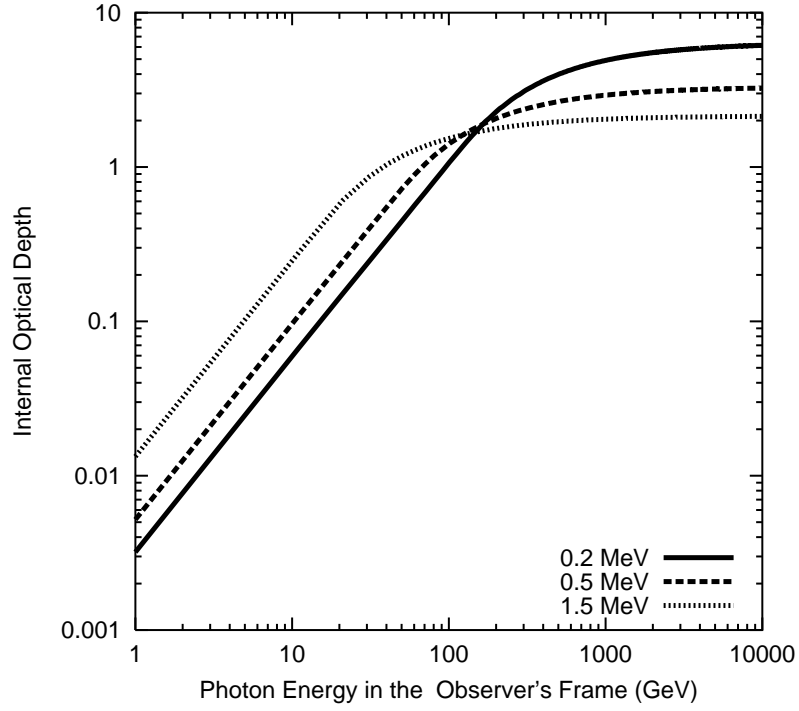


Figure 3: Internal optical depth as a function of the photon's energy in the observer's frame, for various values of the break energy of the observed BATSE spectrum, ϵ_b^{ob} , as indicated. Values taken for other relevant parameters are: $L_{\text{L},51}^{\text{ob}} = 1$, $\beta_l = 1$, $\beta_h = 2.25$, $\Delta t^{\text{ob}} = 0.5 \text{ sec}$, $\Gamma = 300$, and $z = 0.1$.

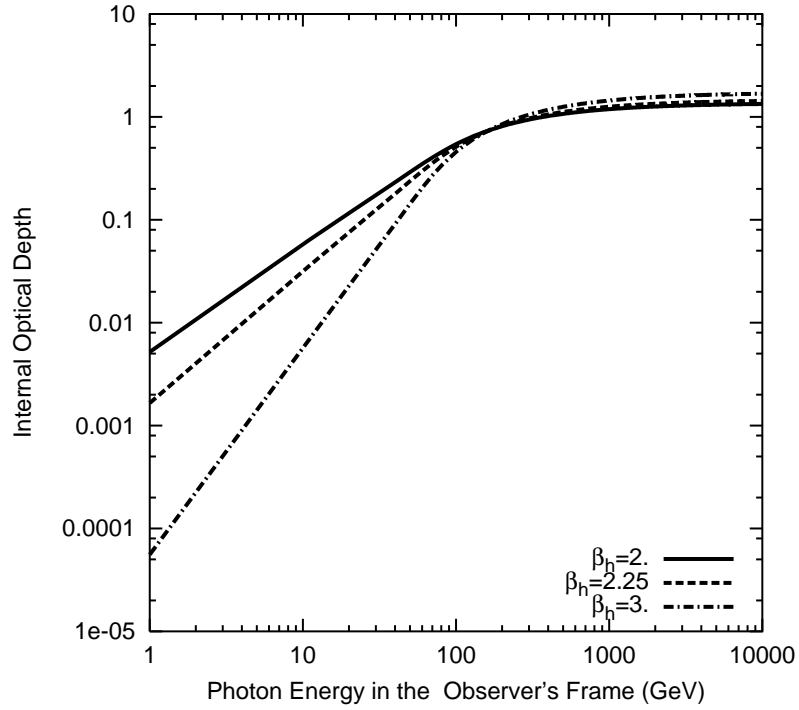


Figure 4: Internal optical depth as a function of the photon's energy in the observer's frame, for various values of β_h as indicated. Values taken for other relevant parameters are: $L_{L,51}^{\text{ob}} = 1$, $\beta_l = 1$, $\epsilon_b^{\text{ob}} = 0.5 \text{ MeV}$, $\Delta t^{\text{ob}} = 0.5 \text{ sec}$, $\Gamma = 400$, and $z = 0.3$.

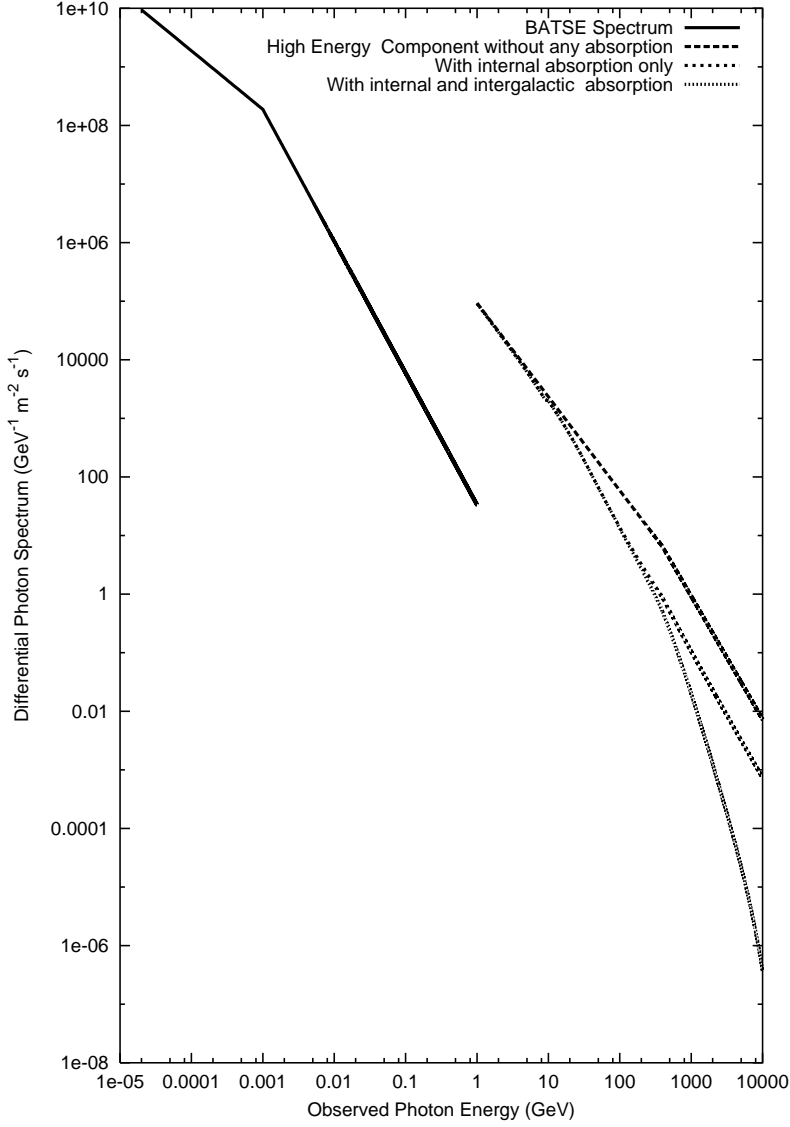


Figure 5: A typical predicted differential spectrum of the high energy component of a GRB due to proton-synchrotron process. The effects of the internal and intergalactic optical depths due to $\gamma\gamma \rightarrow e^+e^-$ process are indicated. The observed low energy “BATSE” spectrum is also shown for comparison. Values taken for the various relevant parameters are: $L_{L,51}^{\text{ob}} = 1$, $\xi_B = 0.5$, $L_H^{\text{lab}} = 10^{54}$ ergs/sec, $\alpha_p = 2.2$, $\beta_l = 1$, $\beta_h = 2.25$, $\epsilon_b^{\text{ob}} = 1$ MeV, $\Delta t^{\text{ob}} = 0.5$ sec, $\Gamma = 300$, and $z = 0.1$.

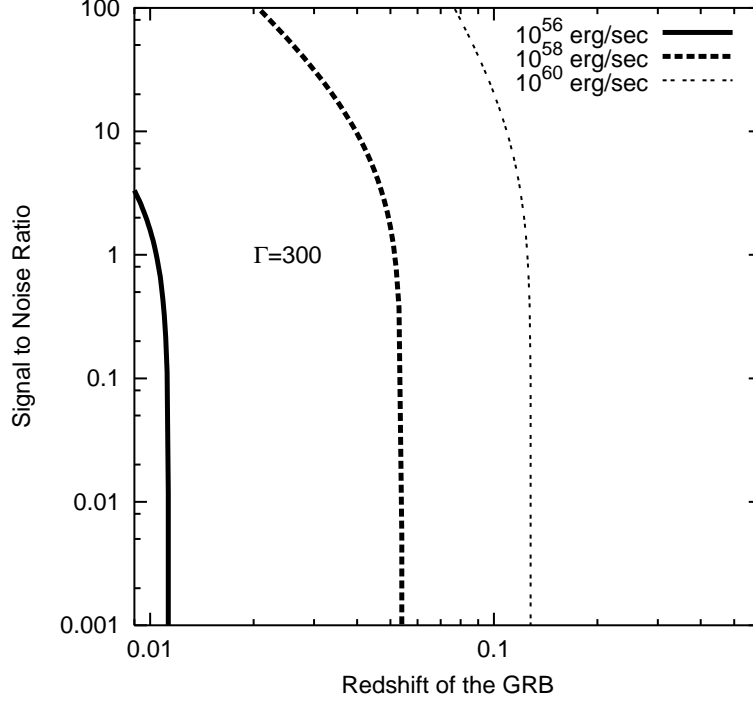


Figure 6: Signal to noise ratio in a ICECUBE class detector as a function of the redshift of the GRB for various values of the luminosity in the high energy component emitted from source, L_H^{lab} , as indicated, including the effects of the internal as well as external (intergalactic) optical depths. The zenith angle of the GRB source is assumed to be zero, and the effective area of the detector for downward-going muons is taken to be $\sim 5 \times 10^5 \text{ m}^2$. The threshold muon energy (at the surface) is taken to be 250 GeV. Values taken for other relevant parameters are: $L_{L,51}^{\text{ob}} = 1$, $\xi_B = 0.5$, $\alpha_p = 2.2$, $\beta_l = 1$, $\beta_h = 2.25$, $\epsilon_b^{\text{ob}} = 1 \text{ MeV}$, $\Delta t^{\text{ob}} = 0.5 \text{ sec}$, $\Gamma = 300$, and $T^{\text{ob}} = (1 + z)10 \text{ sec}$.

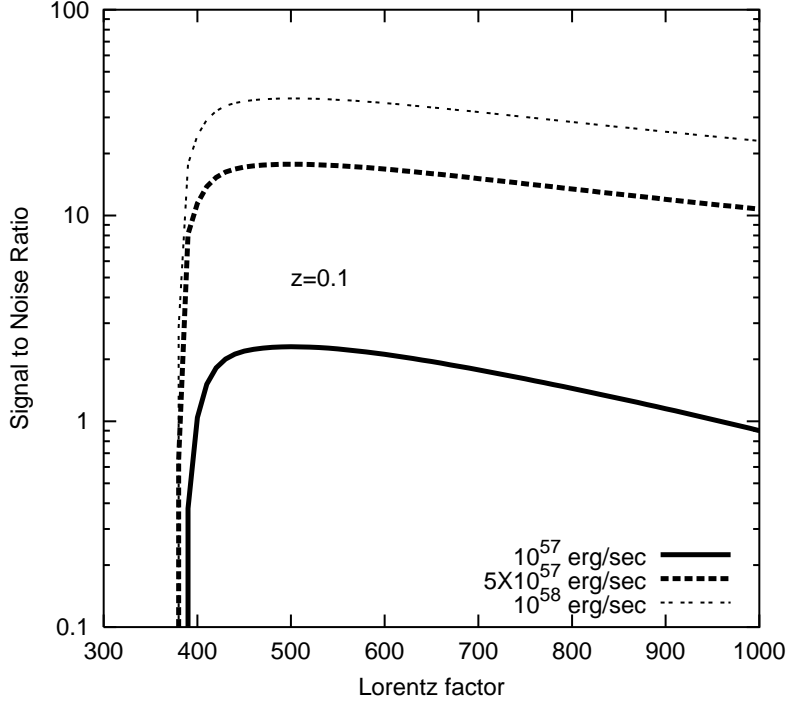


Figure 7: Signal to noise ratio in a ICECUBE class detector as a function of the Lorentz factor Γ of the relativistic outflow characterizing the GRB, for various values of the luminosity in the high energy component emitted from source, L_H^{lab} , as indicated, including the effects of the internal as well as external (intergalactic) optical depths. The zenith angle of the GRB source is assumed to be zero, and the effective area of the detector for downward-going muons is taken to be $\sim 5 \times 10^5 \text{ m}^2$. The threshold muon energy (at the surface) is taken to be 250 GeV. Values taken for other relevant parameters are: $L_{L,51}^{\text{ob}} = 1$, $\xi_B = 0.5$, $\alpha_p = 2.2$, $\beta_l = 1$, $\beta_h = 2.25$, $\epsilon_b^{\text{ob}} = 1 \text{ MeV}$, $\Delta t^{\text{ob}} = 0.5 \text{ sec}$, $z = 0.1$, and $T^{\text{ob}} = (1 + z)10 \text{ sec}$.

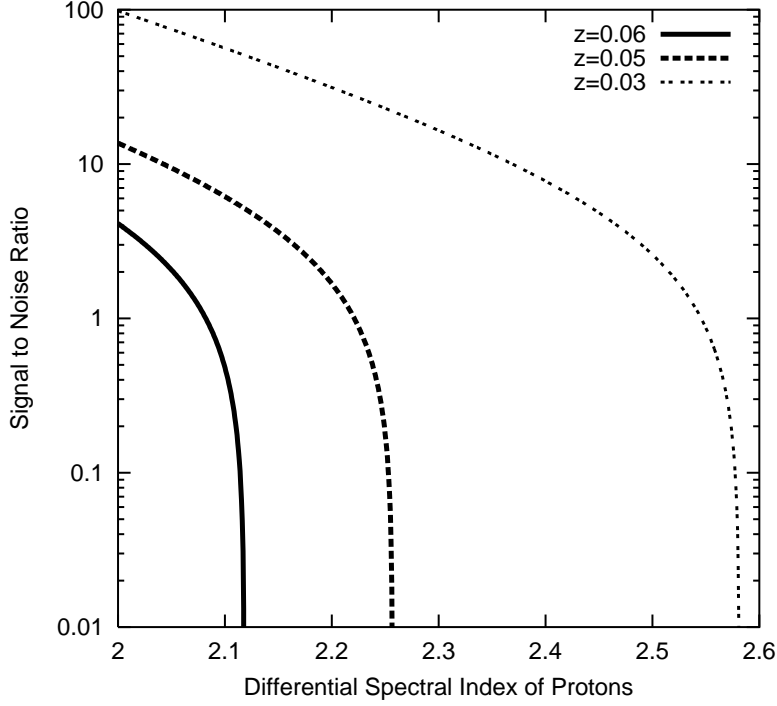


Figure 8: Signal to noise ratio in a ICECUBE class detector as a function of the power-law index (α_p) of the differential spectrum of protons accelerated within the GRB source, for various values of the redshift z of the GRB as indicated, including the effects of the internal as well as external (intergalactic) optical depths. The zenith angle of the GRB source is assumed to be zero, and the effective area of the detector for downward-going muons is taken to be $\sim 5 \times 10^5 \text{ m}^2$. The threshold muon energy (at the surface) is taken to be 250 GeV. Values taken for other relevant parameters are: $L_{\text{L},51}^{\text{ob}} = 1$, $\beta_l = 1$, $\beta_h = 2.25$, $\epsilon_b^{\text{ob}} = 1 \text{ MeV}$, $\xi_B = 0.5$, $\Delta t^{\text{ob}} = 0.5 \text{ sec}$, $\Gamma = 300$, $L_{\text{H}}^{\text{lab}} = 10^{58} \text{ ergs/sec}$, and $T^{\text{ob}} = (1 + z)10 \text{ sec}$.

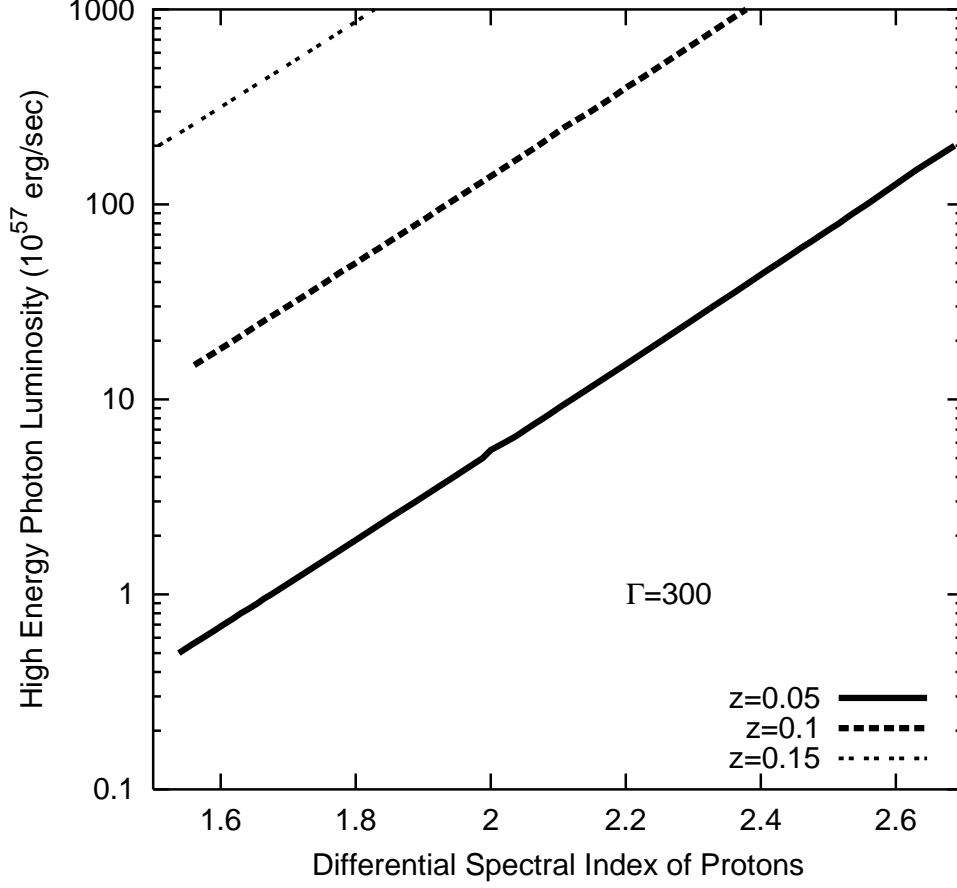


Figure 9: The minimum luminosity in the high energy component, L_H^{lab} , required for detection with a signal to noise ratio of 5 or larger in a ICECUBE class detector, as a function of the power-law index (α_p) of the differential spectrum of protons accelerated within the GRB source, for various values of the redshift z of the GRB as indicated, including the effects of the internal as well as external (intergalactic) optical depths. The zenith angle of the GRB source is assumed to be zero, and the effective area of the detector for downward-going muons is taken to be $\sim 5 \times 10^5 \text{ m}^2$. The threshold muon energy (at the surface) is taken to be 250 GeV. Values taken for other relevant parameters are: $L_{\text{L},51}^{\text{ob}} = 1$, $\beta_l = 1$, $\beta_h = 2.25$, $\epsilon_b^{\text{ob}} = 1 \text{ MeV}$, $\xi_B = 0.5$, $\Delta t^{\text{ob}} = 0.5 \text{ sec}$, $\Gamma = 300$, and $T^{\text{ob}} = (1 + z)10 \text{ sec}$.